

## Observing System Simulation Experiments (OSSEs) to Evaluate the Potential Impact of an Optical Autocovariance Wind Lidar (OAWL) on Numerical Weather Prediction

ROBERT ATLAS,\* ROSS N. HOFFMAN,<sup>+</sup> ZAIZHONG MA,<sup>#</sup> G. DAVID EMMITT,<sup>@</sup> SIDNEY A. WOOD JR.,<sup>@</sup> STEVEN GRECO,<sup>@</sup> SARA TUCKER,<sup>&</sup> LISA BUCCI,<sup>+</sup> BACHIR ANNANE,<sup>+</sup> R. MICHAEL HARDESTY,<sup>\*\*</sup> AND SHIRLEY MURILLO<sup>++</sup>

\* NOAA/Atlantic Oceanographic and Meteorological Laboratory, Miami, Florida

<sup>+</sup> Cooperative Institute for Marine and Atmospheric Studies, Rosenstiel School of Marine and Atmospheric Science, University of Miami, Miami, Florida

<sup>#</sup> Cooperative Institute for Climate and Satellites, University of Maryland, College Park, College Park, Maryland

<sup>@</sup> Simpson Weather Associates, Charlottesville, Virginia

<sup>&</sup> Ball Aerospace and Technologies Corp., Boulder, Colorado

<sup>\*\*</sup> NOAA/Earth System Research Laboratory, Boulder, Colorado

<sup>++</sup> Hurricane Research Division, NOAA/Atlantic Oceanographic and Meteorological Laboratory, Miami, Florida

(Manuscript received 15 February 2015, in final form 27 May 2015)

### ABSTRACT

The potential impact of Doppler wind lidar (DWL) observations from a proposed optical autocovariance wind lidar (OAWL) instrument is quantified in observing system simulation experiments (OSSEs). The OAWL design would provide profiles of useful wind vectors along a ground track to the left of the International Space Station (ISS), which is in a 51.6° inclination low-Earth orbit (LEO). These observations are simulated realistically, accounting for cloud and aerosol distributions inferred from the OSSE nature runs (NRs), and measurement and sampling error sources. The impact of the simulated observations is determined in both global and regional OSSE frameworks. The global OSSE uses the ECMWF T511 NR and the NCEP operational Global Data Assimilation System at T382 resolution. The regional OSSE uses an embedded hurricane NR and the NCEP operational HWRf data assimilation system with outer and inner domains of 9- and 3-km resolution, respectively.


The global OSSE results show improved analyses and forecasts of tropical winds and extratropical geopotential heights. The tropical wind RMSEs are significantly reduced in the analyses and in short-term forecasts. The tropical wind improvement decays as the forecasts lengthen. The regional OSSEs are limited but show some improvements in hurricane track and intensity forecasts.

## 1. Introduction

### a. Winds are arguably the most important variables in the atmosphere

They transport all the other variables of the atmosphere and govern the exchanges of mass, energy, and momentum between the atmosphere and the underlying

ocean and land surfaces. There is a substantial opportunity to improve numerical weather prediction (NWP) by better observing the global wind field (e.g., Atlas et al. 2001). Currently, winds make up a very small fraction of the observations that are used in data assimilation (DA) systems. Many of the winds that are available are created by tracking features in the cloud or water vapor field. These atmospheric motion vectors (AMVs) are very valuable, but they are an indirect measurement and have inherent height uncertainties that make their use somewhat problematic. In contrast Doppler wind lidars (DWLs) directly and very accurately measure the line-of-sight (LOS) wind by observing the Doppler shift in the lidar signal returned by a volume of atmospheric scatterers. While a number of

 Denotes Open Access content.

Corresponding author address: Robert Atlas, NOAA/Atlantic Oceanographic and Meteorological Laboratory, 4301 Rickenbacker Causeway, Miami, FL 33149.  
E-mail: robert.atlas@noaa.gov

DOI: 10.1175/JTECH-D-15-0038.1

© 2015 American Meteorological Society

aircraft-based DWLs have made valuable measurements of winds, the first satellite-based DWL, a European Space Agency (ESA) project named Earth Explorer Atmospheric Dynamics Mission (ADM) Aeolus, is currently planned to launch in 2016. Baker et al. (2014, hereafter B14) provide an excellent description of the need for a DWL, a review of previous impact studies that used both simulated satellite and real-world aircraft-based data, and an overview of instrument concepts and their supporting technologies. Impact experiments with real data, termed observing system experiments (OSEs), are conducted with and without one observing system to quantify the impact of that observing system. Similar experiments with simulated data are termed observing system simulation experiments (OSSEs). In OSSEs a long forecast is taken to be the “truth” or nature run (NR). The present study complements previous DWL OSSEs by examining the impact of a new proposed technology, the optical autocovariance wind lidar (OAWL); observing LOS winds both fore and aft of the satellite; and using a modern operational DA system used by NCEP circa 2012.

*b. There are three basic DWL design concepts that are currently being considered for a space-based mission*

In addition to ESA’s ADM-Aeolus, two maturing U.S. DWL designs—one for OAWL on the International Space Station (ISS) and one for Winds from the ISS for Climate Research (WISSCR)—have been demonstrated to be feasible for deployment on the ISS (refer to supplement of B14). Note that all three of these systems employ both aerosol and molecular scatterers as targets, and that in each case the molecular receiver uses a double-edge Fabry–Pérot interferometer. The Ball Aerospace and Technologies Corp.’s OAWL ISS concept is a dual-direct-detection approach that implements a double-edge receiver for the molecular portion of the atmospheric return, and uses optical autocovariance techniques (Schwiesow and Mayor 1995) for the aerosol portion. The OAWL ISS uses two azimuthally orthogonal-pointed telescopes to observe LOS winds fore and aft on the port (left) side of the ISS. Each telescope is paired with a 355-nm UV laser to provide continuous atmospheric coverage along both lines of sight. A single lidar alternately receives light from each of the two telescopes. All of the OSSEs described in this paper use simulated winds from only the OAWL aerosol receiver (i.e., without the add-on of a double-edge molecular channel). The OAWL sensor is described in section 2a.

*c. Summary of past global OSSEs*

The basic methodology for OSSEs, as modified by Atlas and others in the early 1980s (Atlas et al. 1985a), is

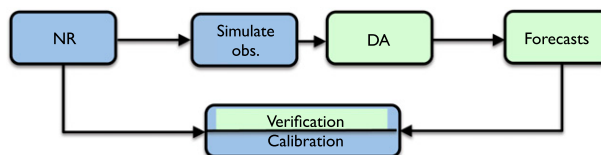


FIG. 1. A top-level view of an OSSE system. For regional OSSEs the NR is taken to be a high-resolution regional (or hurricane) NR, which is embedded in a global NR. Elements taken from the operational DA system are shaded in green.

illustrated in Fig. 1. An OSSE begins with an NR generated by a state-of-the-art atmospheric model. From the NR all currently available observations, as well as any new observations to be evaluated, are simulated. In the experiments reported here, for the wind lidar, a very detailed lidar simulation model is used to estimate the detector response in each range gate and from this the retrieved profile of LOS winds and associated errors. The OSSE proceeds by running DA and forecasts with and without the new observations and verifies the analyses and forecasts against the NR. It is essential that every element of the OSSE process is realistic and that each element is verified and calibrated by comparison with real data OSEs (Atlas 1997).

According to B14, numerous global OSSEs have been conducted both to show the potential of DWLs and to refine proposed designs in trade studies. For example, Atlas et al. (1985a,b) conducted OSSEs to evaluate the relative impact of temperature, wind, and moisture profiles from polar-orbiting satellites. These experiments showed wind data to be more effective than mass data in correcting analysis errors and indicated significant potential for space-based wind profile data to improve numerical weather prediction. Later, Atlas and Riishojgaard (2008) used a 3.5-month-long NR created with the 0.5°-resolution finite-volume general circulation model (fvGCM) and the Goddard Earth Observing System (GEOS), version 3, DA system.

More recent experiments, including several summarized by B14 and those reported here, use the ECMWF T511 (~26-km horizontal resolution) NR (Andersson and Masutani 2010). The most recent of these OSSEs, to assess the potential impact of the proposed Global Wind Observing Sounder (GWOS) mission, were conducted by Riishojgaard et al. (2012) and Ma et al. (2015). The DA system used in the GWOS experiments was the operational NCEP Global Data Assimilation System (GDAS; Kleist et al. 2009) circa 2009. This system included the Global Forecast System (GFS) running at a resolution of T382 (~35-km horizontal resolution). In these experiments, the control experiment included all data used operationally by NCEP in 2005. Riishojgaard

et al. (2012) conducted experiments that when compared to the control experiment 1) removed all radiosonde, pilot balloons, and dropsonde observations; 2) removed all wind observations; and 3) added the GWOS data. Ma et al. (2015) extended the Riishojgaard et al. (2012) study by comparing control and full GWOS configurations to less capable and less costly and power-hungry versions of the GWOS concept, with either one or two lasers on one side of the spacecraft. In contrast to these GWOS experiments, the OAWL experiments reported here use the GDAS circa 2012.

#### *d. OSSE design issues relevant to DWL experiments*

In these experiments great care is taken to accurately simulate the OAWL data (section 3). From the OSSE viewpoint, the critical parameters are the data coverage and the observation errors. For a DWL, data coverage depends on the orbital characteristics (section 2b) and the distribution and characteristics of the aerosols and clouds (section 3e). The simulated errors include measurement and sampling errors (section 3a). For a DWL, instrument engineering and the inclusion of many lidar pulses in a single wind observation can result in very small measurement errors. Further height assignment errors should be insignificant. However, because of the very small horizontal footprint, sampling errors will be present. In addition, the instrument will respond to small-scale variations that are not represented either in the NR or in the DA system.

#### *e. OSSEs for hurricanes*

For hurricanes, NRs derived from global models are not yet of sufficient resolution to depict realistic structure and intensity. So, currently a regional NR is needed. There are two ways to do this. One is to take a regional forecast—say, a 10-day forecast—as the NR for a quick OSSE. But the more rigorous procedure, used here, is to embed a regional model, such as the Weather Research and Forecasting (WRF) Model, within a global NR to generate a consistent regional NR (Zhang and Pu 2010). To our knowledge the 13-day hurricane NR (denoted HNR1; Nolan et al. 2013) is the longest regional NR created and used in this way so far. There are other OSSEs that have examined hurricane forecasting using either global OSSE systems or regional quick OSSE systems. But, as we will see in section 5, the coupled global–regional NR setup provides the novel capability to discriminate impacts due to the use of the new data in the global DA versus in the regional DA on the regional model forecasts.

Earlier OSSEs for hurricanes have included global OSSEs and global quick OSSEs using the NASA fvGCM to evaluate the impact of lidar winds and

hyperspectral sounder observations, primarily on hurricane track prediction. For example, a regional quick OSSE using the MM5 as the NR was used to evaluate the Hurricane Imaging Radiometer (HIRAD; Miller et al. 2008). And a number of investigators have conducted regional quick OSSEs using either the Advanced Research version of WRF (ARW) or the Hurricane WRF (HWRF) Model to produce the NR (e.g., Aksoy et al. 2012).

#### *f. The plan of this paper*

First, the OAWL instrument (section 2) is presented, including its design, nominal orbit, and instrument characteristics. Based on this description, the simulation methodology is detailed in section 3, which includes depictions of the horizontal and vertical data coverage. The global and regional OSSEs that make use of the simulated data are then described and the results are reported for each in sections 4 and 5, respectively. A unique feature of this study is that the regional OSSE is closely linked to the global OSSE. A summary and concluding remarks are given in section 6.

## **2. OAWL description**

### *a. OAWL concept to design*

To profile winds, DWLs measure Doppler frequency shifts of laser light backscattered from aerosols and molecules, as a function of range, along the receiver LOS. The signal backscattered from aerosol particles is spectrally broadened by atmospheric turbulence, while molecular-backscattered returns are also broadened due to the thermal motion of the molecules. Because broadening due to turbulence can be two orders of magnitude smaller than molecular broadening and because, for a given signal level, the precision of the estimate of the Doppler shift improves as bandwidth decreases, the Doppler shift of aerosol-backscattered returns can be determined to a higher precision. Aerosol concentrations vary and low values result in smaller amplitude signals and lower signal-to-noise ratio (SNR). This is often the case at higher altitudes. Measuring winds from both aerosol and molecular backscatter (Emmitt 2000, 2001; Emmitt and Wood 2003, 2011; Hardesty et al. 2005) can thus maximize the availability of wind profiles, at the cost of an additional receiver or receiver channels. In this study only winds simulated from aerosol backscatter are assimilated in our OSSEs. However, section 3 compares the accuracy and coverage of wind from both aerosol and molecular backscatter. Therefore, we briefly describe how the OAWL aerosol sensor can be efficiently combined in an integrated direct-detection system composed of an

OAWL aerosol sensor and a Fabry–Pérot double-edge molecular sensor sharing a single laser. As mentioned in the introduction, such a combined system has been proposed for the ISS platform.

Ball Aerospace and Technologies Corp.'s OAWL is a direct-detection approach to measuring winds from aerosol backscatter with sub-meter-per-second precision (Grund et al. 2009; Grund and Tucker 2011) using optical autocovariance techniques (Schwiesow and Mayor 1995). OAWL is implemented as a modified Mach–Zehnder interferometer (MZI) with cat's-eye mirrors to increase the interferometer's field of view (Grund and Tucker 2011; Tucker and Weimer 2013). The receiver implements a unique high-resolution (1 in  $10^9$ ), field-widened, four-channel MZI (Liu and Kobayashi 1996; Bruneau and Pelon 2003). Like all DWLs, the OAWL receiver operation is ultimately based on measuring small differences in the frequency of backscattered light relative to the frequency of the corresponding outgoing laser pulses. In OAWL, the relative frequency shift is tied to phase shifts in the fringe amplitudes measured by the MZI. In interferometers such as Michelsons or MZIs, optical autocovariance—the correlation of light (mean removed) with a time lagged copy of itself—manifests as the amplitude of a fringe at each detector in the interferometer. Additional information on two- and four-channel MZI Doppler wind lidars and their performance characteristics is provided in the references (Liu and Kobayashi 1996; Bruneau 2001, 2002; Bruneau and Pelon 2003; Bruneau et al. 2004; Tucker and Weimer 2013; Bruneau et al. 2013).

### *b. OSSE system configuration and orbit characteristics*

Like the WISSCR and Aeolus system concepts, the OAWL instrument could be deployed in different low-Earth orbits (LEOs), and in configurations with one, two, and—if funding allowed—four telescopes, to observe LOS winds fore and/or aft, starboard and/or port of the satellite. In the two-telescope ISS configuration, considered for this OSSE study, two telescopes point toward one side (in this case left or port side) of the ISS in order to provide unambiguous information on the  $u$ - and  $v$ -wind components. The ISS is in a  $51.6^\circ$  inclination LEO at a height that varies from 350 to 420 km, but the worst-case scenario of 420 km is considered for all cases here. The OAWL lasers point at azimuth angles of  $45^\circ$  and  $135^\circ$  relative to the spacecraft heading and at  $40^\circ$  off nadir, corresponding to ground relative elevation angles of  $47^\circ$ . Although in reality, regular ISS operations from an ISS module would imply some data gaps (B14s) for any Doppler lidar system, our simulated data assume uninterrupted operation. Observation locations at the ground were

determined with the Analytical Graphics, Inc. (AGI) Systems Tool Kit (STK; see <https://www.agi.com>).

For the notional ISS-based OAWL instrument simulated in this study, the fundamental 1064-nm-wavelength laser pulse energy is 1.2 J, or 0.55 J at the tripled-frequency wavelength of 355 nm (in the ultraviolet). The pulse repetition frequency (PRF) is 50 Hz. The telescope aperture diameter is 0.7 m ( $<0.37\text{ m}^2$  effective area when the telescope obscuration is taken into account).

### **3. OAWL-simulated data**

To generate simulated DWL observations for the OSSE, a radiometric model is combined with a complete description of the relevant atmospheric state variables to estimate the amount of backscatter laser energy detected by the instrument and to estimate the associated noise. The accuracy of a DWL estimate depends on the number of backscattered lidar photons and the number of scattered solar photons received by the instrument. LOS winds estimated for individual pulses are noisy and representative of a very small volume with a horizontal extent of  $O(10\text{ m})^2$ . Therefore, each DWL observation—that is, each profile of LOS winds—is determined from a number of consecutive pulses. In this study, each OAWL observation corresponds to 600 pulses, which corresponds to 12 s of operation at 50 Hz, during which time the satellite ground track advances by 80 km. LOS winds estimated in this way may not be representative of the  $\sim 80\text{ km} \times 80\text{ km}$  volume containing the line of pulses. This is termed sampling error.

In simulating the OAWL observations, errors are added due to measurement error and sampling error. For measurement error the number of photons received is effectively determined pulse by pulse. In practice, for each observation location, a single representative lidar pulse and solar beam are traced to the ground and back to the instrument assuming clear conditions, and as the pulse is traced level by level through the atmosphere, molecular and aerosol absorption and scattering in each layer is determined. The backscattered energy from each atmospheric layer (equivalently, each time gate) is saved and used in determining the cloud-affected signal and noise for each pulse.

Various cloud types along the atmospheric column will contribute both backscatter and extinction (i.e., attenuation via absorption and scattering in other directions). The specific optical properties for each atmospheric layer are specified from a combination of the NR and statistical databases. To account for cloud porosity, the saved quantities for the representative pulse are then applied to each group of pulses having the

same cloud parameters and the measurement noise for the group is estimated. Finally, the group measurement noise values, weighted by the size of the group, are combined in an RMS sense to produce the measurement noise for the OAWL observation.

The strength of the received signal, the ratio between aerosol- and molecular-backscattered returns, and the scattered solar radiation impact the estimated measurement error. A comprehensive engineering model, similar in the level of detail and complexity to models for other DWLs (e.g., [Frehlich 2000, 2001, 2004](#)), is used for this purpose. Sampling noise is then added to the measurement error to get the total observation error.

Within a DA system an additional “representativeness” error is included in the estimated observation error standard deviation to account for differences in the scales measured by the DWL and the scales represented by the atmospheric model. Representativeness error is an expression of how well the simulated DWL observations represent the winds on scales resolved by the numerical models being used in the OSSEs and should include every source of variability that affects the observation in reality, that is, either not included or incorrectly modeled in the DA system. For DWL the main source of representativeness error is the variability of small scales of motion, observed by the DWL but not represented in the DA system. The sources of representativeness error are really limitations of the DA system, but they must be assigned to the observations for the purpose of DA. Without representativeness error, the DA system would overfit the DWL observations.

OAWL winds are simulated using the Doppler Lidar Simulation Model (DLSM) described by [Wood et al. \(2000, 2001\)](#) and [Emmitt and Wood \(1996\)](#). Both direct-molecular- and direct-aerosol-detection wind lidar returns were simulated for both nominal and enhanced aerosol conditions. In the global (regional) OSSEs described below, only the aerosol OAWL LOS winds for background (enhanced) aerosol conditions were assimilated. In this section we present some results for quality and data coverage for LOS winds from four configurations—for both the OAWL and double-edge technique LOS winds, in both background and enhanced aerosol conditions. Plans for OSSEs using various combinations of simulated winds were made, but resources limited the number of OSSEs that were actually carried out. However, results presented in this section do quantify the accuracy and coverage of the four configurations.

#### *a. Simulation methodology*

The DLSM is a comprehensive lidar simulation system that allows for a variety of DWL or other lidar instruments hosted by either satellite or aircraft platforms

and that permits the use of many standard weather model datasets to describe the atmosphere. The DLSM provides several different signal processing options. The atmosphere definition includes cloud and aerosol optical properties, including cloud porosity. [Figure 2](#) gives a schematic depiction of the DLSM. A number of options exist for defining the instrument (laser frequency, power, coherent and/or direct detectors, telescope scanning strategy, observing management strategy), platform, atmosphere, signal processing, and error processing. Once the options are chosen and the appropriate values assigned, the DLSM procedure includes the following steps:

- 1) Use the instrument scanning and observing management parameters and the platform parameters to define the geometry of each lidar observation.
- 2) Evaluate the atmosphere along the representative pulse path.
- 3) Calculate the error-free observations of LOS wind using the signal processing algorithms.
- 4) Add appropriate errors to the error-free observations, based on the error options chosen and the associated parameters.

#### *b. Cloud effects*

One of the most critical aspects of the DLSM is the representation of clouds along the line of sight of each pulse. This cloud accounting determines which levels are observed. The challenge is to fully specify a reasonable representation of cloud parameters, from the satellite viewpoint, that are consistent with the gridpoint values from the NR. These cloud parameters include backscatter, attenuation, cloud porosity, multilayering, and multiple-scattering effect. The DLSM uses the following procedure: First, NR cloud fractions  $< 0.05$  are treated as clear. Second, if there is a cloud present, then the cloud is considered opaque unless the liquid water content is less than a threshold ( $0.05 \text{ g kg}^{-1}$  in this study) and the air temperature is less than a threshold ( $273 \text{ K}$ ), in which case the cloud is considered to be a cirrus cloud. If the cloud is judged to be cirrus, then the fraction is assumed to be 1.0, while the NR cirrus cloud amount is used to scale the cloud optical depth. Thus, DWL pulses intercepted by cirrus always yield returns from the cloud, as well as attenuated returns from lower levels. From a computational perspective, cirrus clouds are treated as an aerosol layer. If the cloud is opaque and it is the first level with an opaque cloud, then the fractional amount is used to randomly determine whether the pulse intercepts the cloud. If the pulse intercepts the cloud, then it produces a cloud return and no further returns from below. If not, then it produces an aerosol/molecular return and the pulse continues to be traced

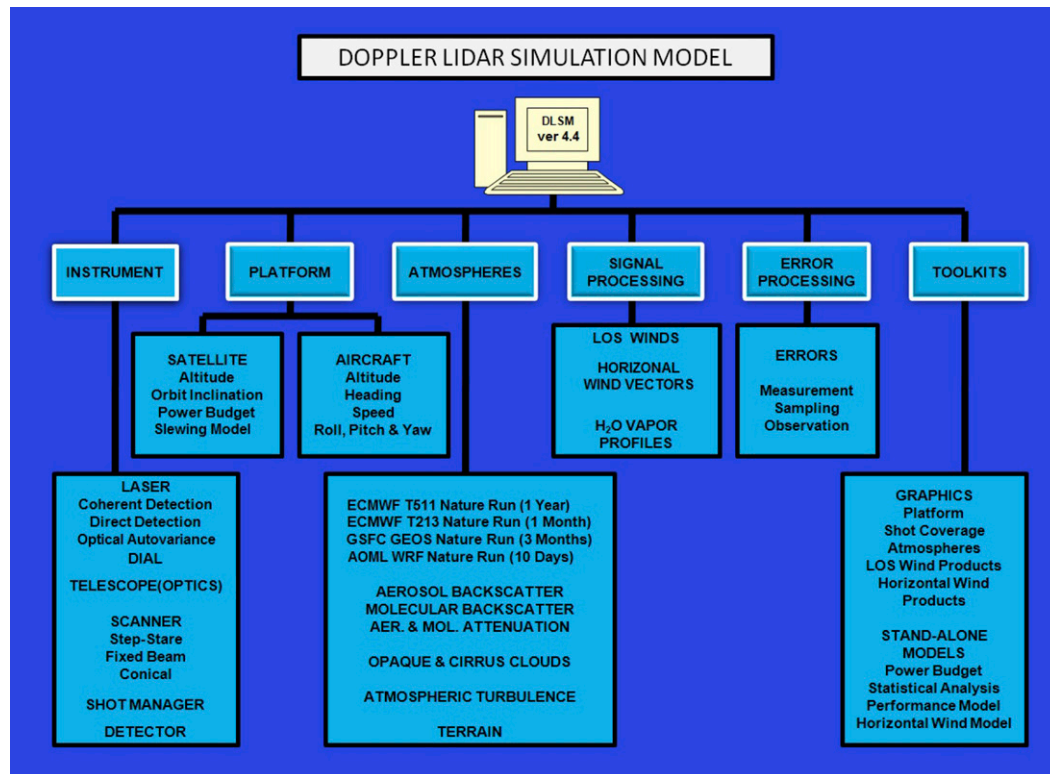


FIG. 2. Functional schematic of the DLSM used to simulate observations. Refer to the text for explanation.

downward to produce additional returns. For subsequent cloud levels, the interaction depends upon whether the cloud is contiguous. If contiguous, then maximum overlap is assumed. If the cloud is non-contiguous, then random overlap is assumed.

### c. Aerosol properties and distribution

In an OSSE the principal atmospheric variables (i.e., temperature, wind, humidity, cloud parameters) are taken from the NR. However, the NRs used in this study do not include aerosols and understate cirrus coverage.

Aerosol backscatter from the atmosphere can vary over several orders of magnitude and depend upon altitude, latitude, and season. The DLSM includes background and enhanced optical property databases based on the surveys of the Global Backscatter Experiment (GLOBE), the South Atlantic Backscatter Lidar Experiment (SABLE), and the Global Atmospheric Backscatter Lidar Experiment (GABLE), as well as from the Air Force Geophysics Laboratory (AFGL) Fast Atmospheric Signature Code (FASCODE). Backscatter databases are generated for the potential DWL wavelengths of 355, 532, 1065, and 2052 nm. These aerosol optical properties follow Emmitt et al. (2001). While the precise backscatter coefficients cannot be known, having a common scattering target with

internally consistent backscatter wavelength dependence enables meaningful “equal resource/equal target” comparisons of DWL concepts. Figure 3 shows the 355-nm background and enhanced backscatter profiles. The DLSM has previously used either the median profile or a normal random number is used to scale the median profile at each observation location by adding  $\eta\sigma(z)$  to the median profile in log space. In these previous applications, a single random draw  $\eta$  from a zero mean, unit variance, normal distribution is used for each location and  $\sigma(z)$  is the profile of standard deviation in log space depicted in Fig. 3.

In the global OSSEs reported here, a somewhat different approach is used. At each location and at every level,  $\eta = \mathcal{N}^{-1}(\text{RH})$ , where  $\mathcal{N}^{-1}$  is the inverse of the normal cumulative distribution function (cdf) and RH is the relative humidity expressed as a fraction and clipped to the interval [0.01, 0.99]. In this way the DLSM uses the NR humidity fields to organize the 3D aerosol scatter and backscatter optical properties. This approach is better than the previous approaches in that RH and aerosol both vary on small length scales and some aerosols increase in size with RH. In the current experiments, one further adjustment was made. Since the planetary boundary layer (PBL) is a first-order concentrator of aerosols generated at the earth’s surface,

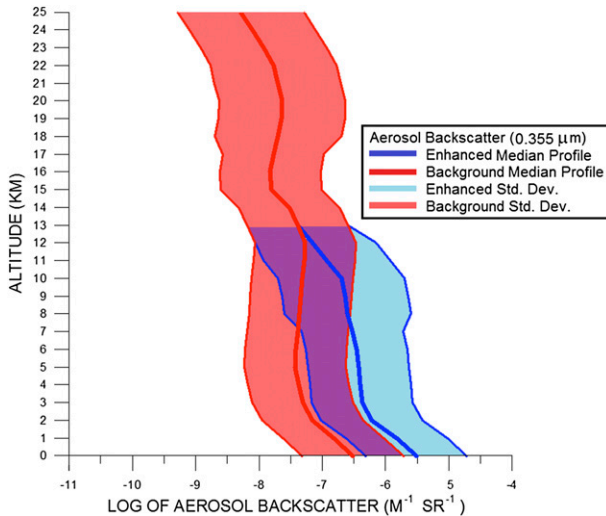


FIG. 3. Median and plus/minus one standard deviation of aerosol backscatter [ $\log(\text{m}^{-1} \text{sr}^{-1})$ ] as a function of altitude (km) at 355 nm for background (red) and enhanced (blue) conditions based on Emmitt et al. (2001).

aerosols are well mixed in the PBL with a rapid vertical transition to the background (or enhanced) profiles above the top of the PBL. Therefore, the RH-generated aerosols in the PBL are replaced with a constant concentration in the PBL that conserves the total column aerosol mass. The archived PBL depth from the NR is used in this calculation. Examples of the results of estimating aerosol from RH in the midtroposphere and in the PBL are shown in Fig. 4. For closure, Fig. 5 shows the backscatter distribution obtained from sampling the aerosol backscatter from the T511 NR for 24 h at the OAWL observation locations. The similarity of the distributions in Figs. 3 and 5 demonstrates the consistency of this approach.

#### d. Error methodology

While the OAWL instrument intrinsic errors (i.e., measurement error) for LOS wind and height assignment are small, for the purpose of DA, there are two other sources of error that must be accounted for, which are commonly called the sampling error and the representativeness error. Simulated observation errors include the measurement and sampling errors. These are taken to be uncorrelated. The methodology of Wood et al. (2000) includes a detailed model of the measurement error propagation onto the final error of the wind product. The simulated observation error (measurement plus sampling error) is determined from basic instrument characteristics and atmospheric physics within the illuminated volumes. In the case of direct-detection systems like OAWL, measurement precision is proportional to the number of photons available to make a

LOS estimate and the variability of the winds within the sampling volumes.

In the experiments reported here, the DLSSM estimates the wind variance on the subgrid scale of the model as 20% of the mean model wind speed on the  $9 \times 9 \times 9$  cube of surrounding grid points. Analyses of rawinsonde and microwave sounder profiles support the use of the 20% rule. For OAWL simulations, most of the simulated LOS uncertainty is due to measurement uncertainty, not sampling uncertainty due to the large number of samples.

#### e. Coverage: Horizontal, vertical

Simulations of OAWL winds were created by the DLSSM for the period 29 July–11 August 2005 for the T511 NR. Examples of the coverage and accuracies of the simulated OAWL winds for background conditions are shown in Fig. 6 for a typical 24-h period. The double-edge detector (right) obtains close to 100% coverage in the upper troposphere, and very good coverage in the PBL except where thick clouds exist, such as in the intertropical convergence zone (ITCZ). In contrast the OAWL detector has somewhat poorer coverage but improved accuracy.

For the same 24-h period, the yield of observations by layer and quality is shown in Fig. 7 for both background (top) and enhanced (bottom) aerosol conditions and for both the OAWL (left) and double-edge (right) detectors. These performance diagrams, which have been used for many years in the DWL community, serve as a good way to compare the quality and distribution of LOS winds from different DWL concepts. Each diagram displays the percentage of time that a lidar system can make useful measurements, taking into account the vertical profile of aerosols, molecules, clouds and cirrus clouds, and the percentage of time that no measurement is made due to overlying opaque clouds.

In the present case, comparing OAWL to the double-edge performance, we see that as in Fig. 6, the molecular (double edge) observations are more widespread but less accurate than the aerosol observations. Comparing the performance for the background and enhanced aerosol conditions, we see, as expected, the enhanced aerosol observation yield increases. However, the additional aerosol scattering translates into reduced pulse energy in the lower atmosphere and a reduced molecular (double edge) observation yield.

## 4. Global OSSEs

### a. Global NR

The global NR used here is based on the operational T511 91-level ECMWF forecast model (version c31r1)

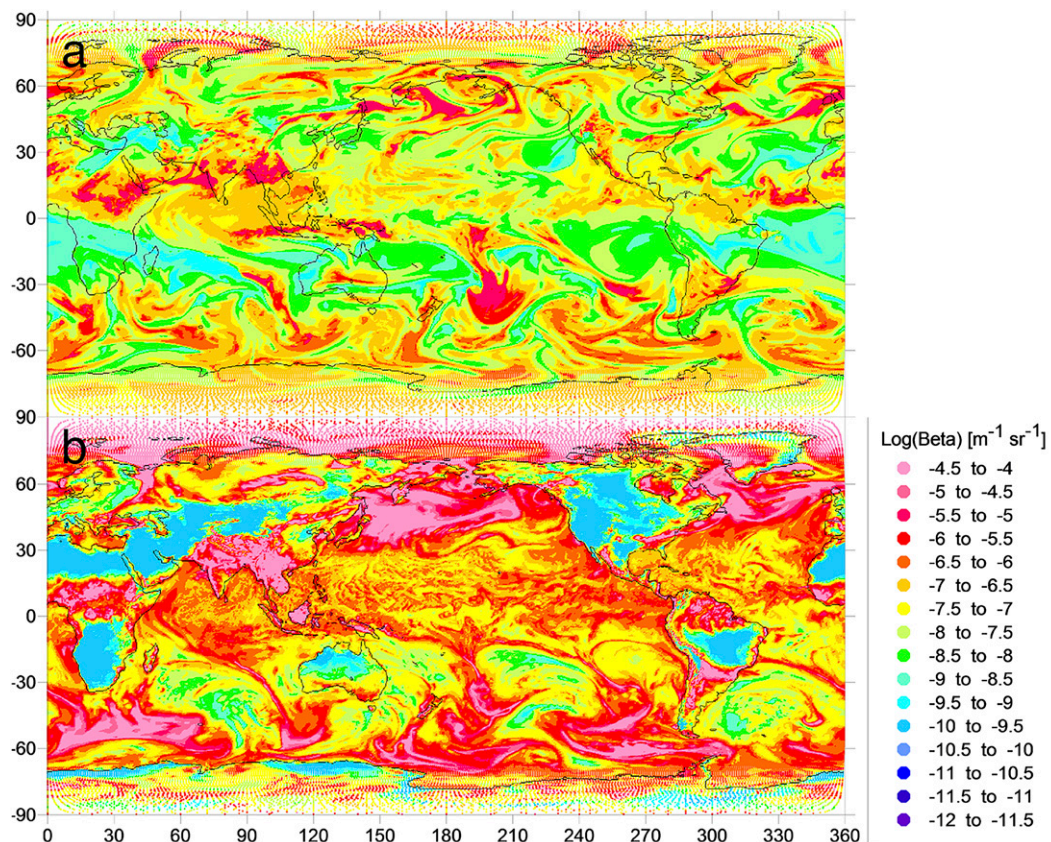


FIG. 4. Estimated aerosol backscatter [ $\log(\text{m}^{-1} \text{sr}^{-1})$ ] at 355 nm for the background conditions at (a) 500 and (b) 1000 hPa. The RH of the T511 NR at 0000 UTC 1 Jul 2005 was used as described in the text.

and will be referred to here as the T511 NR. The T511 NR is described by [Andersson and Masutani \(2010\)](#) and is a free-running forecast from 1200 UTC 1 May 2005 to 1200 UTC 1 June 2006 that used observed sea surface temperature (SST) and sea ice. Evaluations of the T511 NR are generally satisfactory (e.g., [Reale et al. 2007](#); [McCarty et al. 2012](#)) and this NR has been used in several previously reported studies (e.g., [Riishojgaard et al. 2012](#); [Privé et al. 2013a,b, 2014a,b](#); [Ma et al. 2015](#)).

#### b. Experimental setup: CTRL, OAWL

Results from two experiments are described here.

- 1) *CTRL*: a control DA experiment in which the observations of each type are simulated to match the locations and times (but with the year shifted to 2005) of the observations of that type, which were actually assimilated in the 2012 operational GDAS.
- 2) *OAWL*: a DA experiment that parallels CTRL but with simulated OAWL data added.

The simulated satellite data are listed in [Table 1](#).

The global OSSEs use the 2012 version of the operational NCEP GDAS but at a reduced horizontal

resolution of T382. The T382 horizontal resolution was used operationally from 1200 UTC 31 May 2005 until 1200 UTC 28 July 2010, when the operational resolution was changed to T574, which remained the operational resolution until 1200 UTC 14 January 2015. All of these configurations use 64 vertical layers. The GDAS has two main components: the Gridpoint Statistical Interpolation Analysis System (GSI), a 3D variational analysis system that assimilates a wide range of data types and which includes a variational bias correction for radiances; and the GFS, which is a global spectral hydrostatic primitive equations forecast model. The GDAS cycles the GSI and GFS every 6 h with  $\pm 3$  h data windows centered on the synoptic times of 0000, 0600, 1200, and 1800 UTC. Every 6 h, the GFS model is integrated to 9 h to allow for calculating the innovations [observation minus background ( $O - B$ )] using the background interpolated to the observation time, in the so-called first guess at the appropriate time (FGAT) procedure. Each day at 0000 UTC, a 7-day (168 h) GFS forecast is made.

In the OAWL experiment, simulated wind profiles are assimilated as a new type of observation, which measures



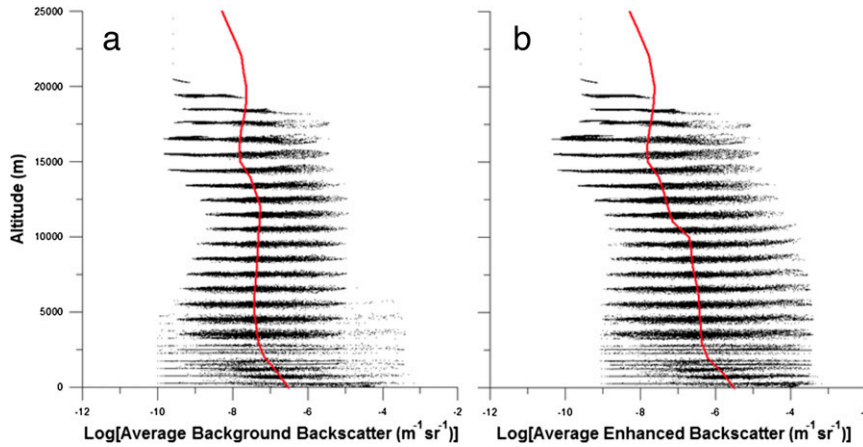


FIG. 5. Simulated OAWL aerosol backscatter [ $\log(\text{m}^{-1} \text{sr}^{-1})$ ] as a function of altitude (m) from the T511 NR for the 24-h period beginning 2100 UTC 28 Jul 2005 for (a) background and (b) enhanced conditions. The heavy red lines are the medians from Fig. 3.

only the LOS projection of the horizontal wind vector. The LOS operator (e.g., Ma et al. 2015) is essentially the same as a standard wind profile operator, with a final additional step of projecting the wind vector onto the LOS, and the requirement to store the LOS geometry in the observation data structure. Within the GSI, observation error statistics for LOS winds have the same vertical structure as radiosonde winds but are reduced by a factor of 0.75.

In the CTRL and OAWL experiments, no observation errors were specified for the conventional observations (i.e., perfect observations) following Riishojgaard et al. (2012). Observation errors for the

OAWL observations were calculated using the procedures described in section 3d. Experiments such as these, with perfect CTRL observations and realistic errors for a proposed instrument, are expected to set a lower bound on the impact of the proposed instrument since the usefulness of the CTRL observations can only be diminished by adding errors.

c. Results

The CTRL and OAWL experiments begin 1800 UTC 28 July 2005 and end 0000 UTC 27 August 2005. After the DA is complete, forecasts for each experiment were initialized at each 0000 UTC and verified against

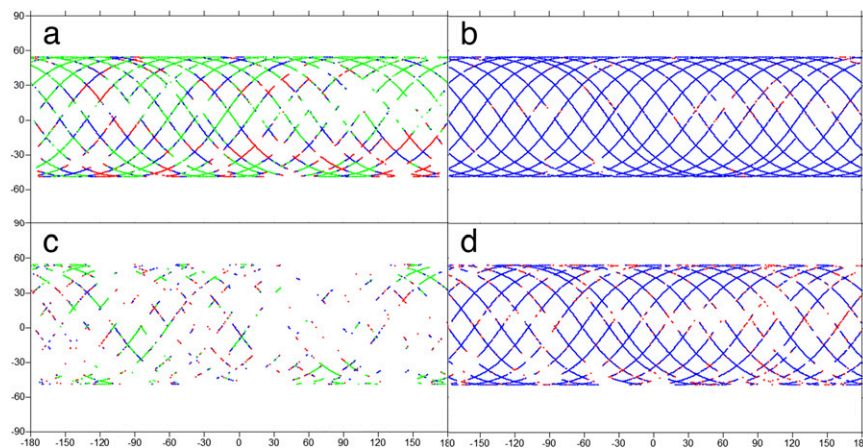


FIG. 6. (a),(b) Sampling patterns and accuracy for the OAWL LOS winds simulated from the T511 NR for background conditions at 11 km and (c),(d) within the marine boundary layer for the 24-h period beginning 2100 UTC 28 Jul 2005 for (a),(c) an OAWL detector and (b),(d) a double-edge detector. The minimum spacing between LOS wind estimates is 80 km. The RMSE of the horizontal projection of the LOS velocity is indicated in green for values between 0 and  $1 \text{ m s}^{-1}$ , in blue for values between 1 and  $3 \text{ m s}^{-1}$ , and in red for values between 3 and  $5 \text{ m s}^{-1}$ .

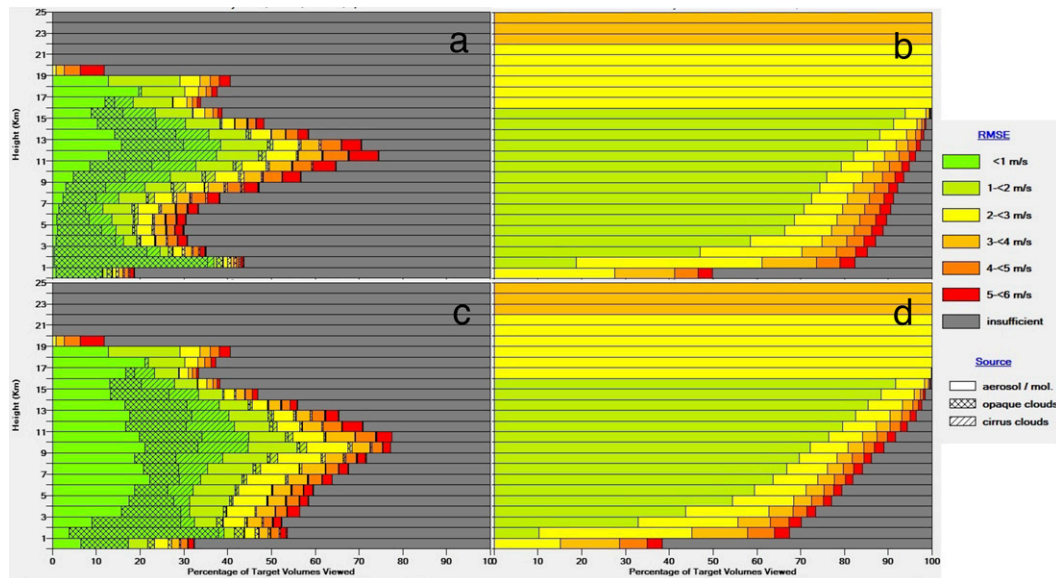


FIG. 7. Performance profiles for background aerosol conditions for (a) the OAWL and (b) the double-edge detectors for the T511 NR during the 24-h period beginning 2100 UTC 28 Jul 2005. These plots should be viewed as stacked histograms of the RMSE of the horizontal projection of the LOS velocity. The length of each color bar at any level gives the fraction of all attempts at that level with RMSE values within the range given for that color in the legend on the right. The uncertainty estimates include the effects of aerosols, sample scale turbulence, opaque clouds, and cirrus clouds. (c),(d) The corresponding performance profiles for enhanced aerosol conditions.

the NR. Both forecasts and NR were interpolated to  $2.5^\circ \times 2.5^\circ$  resolution before the statistics were calculated. Forecast statistical results are for the period 7–27 August 2005, which eliminates the first 8 days of the experiments, by which time there should be no transients in the DA system. Note that the wind RMSE is the vector wind RMSE, and that the vector wind mean-square error (MSE) is equal to the sum of the  $u$ - and  $v$ -component MSE.

Globally, the analysis misfit to the observations (observation minus analysis) and the observation innovations (observation minus background) for the DWL shown in Fig. 8 both decrease in size during the first 48 h of the OAWL experiment and are then steady at values of approximately  $1.0$  and  $2.0 \text{ m s}^{-1}$ , respectively, for almost 2 weeks. Over the last 2 weeks of the experiment, the observation innovations decrease noticeably to  $1.8$ – $1.9 \text{ m s}^{-1}$  and the analysis fit to the observations improves slightly.

### 1) TROPICAL WINDS

The evolution of the RMS of the analysis errors [analysis minus truth ( $A - T$ ), where  $T$  is the truth as given by the T511 NR] in the tropics ( $20^\circ\text{S}$ – $20^\circ\text{N}$ ) at 200 and 850 hPa are compared for CTRL and OAWL in Fig. 9. Within 2 days, transients in these statistics are no longer apparent and the OAWL analyses are substantially closer to the truth, with the RMSE being reduced from approximately 5.0 to approximately

$3.25 \text{ m s}^{-1}$  at 200 hPa and with a somewhat smaller percentage-wise reduction of 20% at 850 hPa. The impact of the OAWL data on the analysis of tropical winds is positive for almost all synoptic times during the experiment near the surface and is uniformly positive for all levels from 850 hPa and above (not shown).

The improvements from the analyses decay during the 7-day forecast period (Fig. 10, top panels) but remain significant at the 95th percentile out to at least 6 days at these two levels (Fig. 10, bottom panels). The decrease in skill with forecast length shown in Fig. 10 is similar to comparable impacts reported by Riishojgaard et al. (2012) and Ma et al. (2015). The variation with pressure level from 1000 to 10 hPa is shown in Fig. 11. The largest RMSEs are near 150 and 20 hPa. The growth of errors above 50 hPa is slow and suggests that the analysis of tropical wind above this level has little information content. For this statistic, the impact of OAWL is uniformly positive out to day 6.

### 2) EXTRATROPICAL GEOPOTENTIAL HEIGHTS

In contrast to the tropical winds, the extratropical geopotential height forecast impact is small initially [until day 3 in the Northern Hemisphere (NH) and until day 2 in the Southern Hemisphere (SH)] and then improves during the forecast period (Fig. 12, top panels), and this improvement is significant for the most part at the 95th percentile (Fig. 12, bottom panels).

TABLE 1. Satellite data sources. Instruments, locations, and times match those of data actually assimilated in the 2012 operational GDAS. All of these satellite observations are assimilated as radiances, except the last three listed, which are assimilated as refractivities (GPS RO), 10-m wind vectors (ASCAT), and 10-m wind speeds (WindSat). The platform names that are given as acronyms in the table include Constellation Observing System for Meteorology, Ionosphere and Climate (COSMIC), Defense Meteorological Satellite Program (DMSP), Meteosat Second Generation (MSG), and *Suomi–National Polar-Orbiting Partnership (Suomi-NPP)*.

Instrument	Acronym definition	Platform(s)
AIRS	Atmospheric Infrared Sounder	<i>Aqua</i>
AMSU-A	Advanced Microwave Sounding Unit-A	<i>Aqua; MetOp-A; NOAA-15, -16, -17, -18, -19</i>
AMSU-B	Advanced Microwave Sounding Unit-B	<i>NOAA-15, -16, -17</i>
ATMS	Advanced Technology Microwave Sounder	<i>Suomi-NPP</i>
CrIS	Cross-Track Infrared Sounder	<i>Suomi-NPP</i>
GOES Sounder	Geostationary Operational Environmental Satellite	<i>GOES-10, -12, -13</i>
HIRS-2	High-Resolution Infrared Radiation Sounder-2	<i>NOAA-14</i>
HIRS-3	High-Resolution Infrared Radiation Sounder-3	<i>NOAA-15, -16, -17</i>
HIRS-4	High-Resolution Infrared Radiation Sounder-4	<i>MetOp-A; NOAA-18, -19</i>
HSB	Humidity Sounder for Brazil	<i>Aqua</i>
IASI	Infrared Atmospheric Sounding Interferometer	<i>MetOp-A</i>
MHS	Microwave Humidity Sounder	<i>MetOp-A; NOAA-18, -19</i>
MSU	Microwave Sounding Unit	<i>NOAA-14</i>
SEVIRI	Spinning Enhanced Visible and Infrared Imager	MSG
SSM/IS	Special Sensor Microwave Imager/Sounder	<i>DMSP F16</i>
GPS RO	Global positioning system radio occultation	COSMIC
ASCAT	Advanced Scatterometer	<i>MetOp-A</i>
WindSat	Space-Based Multifrequency Polarimetric Microwave Radiometer	<i>Coriolis</i>

Figure 13 shows the variation of the 500-hPa geopotential height forecast anomaly correlation coefficient (ACC) for the individual forecasts for the NH and SH. The CTRL panels show that the ACC varies more as the forecast length increases, with some forecasts being substantially better than others at longer lead times. For example, the 7-day forecast verifying on 17 August 2005 has a NH ACC > 0.8, while the 7-day forecast verifying on 11 August 2005 has an NH ACC < 0.6. Also, forecasts in the NH are somewhat better than in the SH. The OAWL minus CTRL panels show a generally positive impact due to OAWL, and more so in the SH. Note that in this display, statistics for a single forecast fall along diagonal lines.

As noted in B14 (pp. 549, 550), “the overall rate of progress of NWP skill over the last 10–20 years has generally ranged from 0.5 to 1 point [in this metric] annually due to a combination of factors. . . . Typically, a contribution that can be attributed to a specific new observing system is generally modest. In that context, the large magnitude of the impact of the DWL is exceedingly rare.”

### 3) SYNOPTIC EVALUATION

Figure 14 shows that the differences in the 7-day 500-hPa geopotential height can be as large as several hundred meters and that these differences are on the scale of synoptic systems. Difference patterns for other forecasts are similar. Nevertheless, at this forecast range, CTRL and OAWL are more similar to each other than either is

to the NR, as can be seen in the displacements of the main troughs and ridges in the 5100-m geopotential height contour.

## 5. Preliminary HWRF OSSEs

In the experiments described in this section, a high-resolution WRF NR was embedded in the T511 NR. Regional-scale DA for hurricanes is quickly evolving, and the newest HWRF system is improved over the 2012 version used in these experiments. Further, the results reported are preliminary and are based on a small sample of runs. However, the experimental setup of coordinated global and regional NRs is, we believe, unique and original, and it allows us to explore the impact of the OAWL data on hurricane forecasts by 1) assimilation on the global scale through improved HWRF initial conditions (IC) and boundary conditions (BC), 2) assimilation on the regional scale through improved HWRF IC, and 3) the combined action of global and regional assimilation.

### a. NR

The NR used in these hurricane OSSEs, called HNR1, was developed with the goal of enabling research on assimilating radiances and retrievals from infrared and microwave instruments in both clear and cloudy conditions. As described in detail in Nolan et al. (2013), HNR1 was created by embedding a WRF Model run in

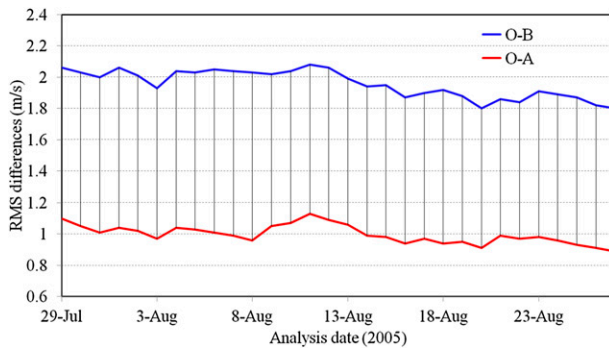


FIG. 8. The RMS O – A ( $\text{m s}^{-1}$ , red) and the RMS O – B ( $\text{m s}^{-1}$ , blue) for OAWL lidar wind observations assimilated from 29 Jul to 27 Aug 2005.

the T511 NR. The period of the HNR1 is from 0000 UTC 29 July 2005 to 0000 UTC 11 August 2005. HNR1 uses nested grids of 27-, 9-, 3-, and 1-km resolution with  $240 \times 160$ ,  $120 \times 120$ ,  $240 \times 240$ , and  $480 \times 480$  grid points, respectively. The inner three grids move with the hurricane. In the vertical, 60 layers are used with a model top at 50 hPa. The HNR1 uses the WRF double-moment 6-class (WDM6) cloud physics, the Rapid Radiative Transfer Model for GCMs (RRTMG) for both thermal and solar radiative transfer, and the Yonsei PBL parameterization. There is no convective parameterization on the 1- and 3-km grids; Kain–Fritsch convective parameterization is used on the outer grids. HNR1 includes a mixed layer ocean. This is sufficient to capture the first-order effect of the hurricane on the SST.

The greater resolution and more sophisticated physical parameterizations used in HNR1 creates a hurricane that, while having a similar track, is much more intense than in the T511 NR (Fig. 15). In order that the HNR1 closely matches the T511 NR, the outer 27-km-grid winds, temperature, and humidity variables are nudged toward the T511 NR interpolated to the 27-km WRF grid using four-dimensional data assimilation (FDDA; Stauffer and Seaman 1990; Stauffer et al. 1991). The least amount of nudging necessary to match the hurricane tracks in the two NRs was used. The similarity in the track of this hurricane in the two NRs is shown in Fig. 15a. Thanks to this nudging procedure, it is possible to reuse some of the simulated observations from the global OSSEs in the HWRF OSSEs. The intensification, shown in terms of sea level pressure (SLP) in Fig. 15b, for the regional NR (blue) is much stronger than for the global NR (black). In the regional NR, the hurricane undergoes rapid intensification centered on day 7 (4 August 2005). Further, the structure is much more realistic in the regional WRF NR than in the ECMWF T511 global NR. For example, Figs. 15c and 15d show that clouds and precipitation in HNR1 are much more realistic in terms of scale and intensity.

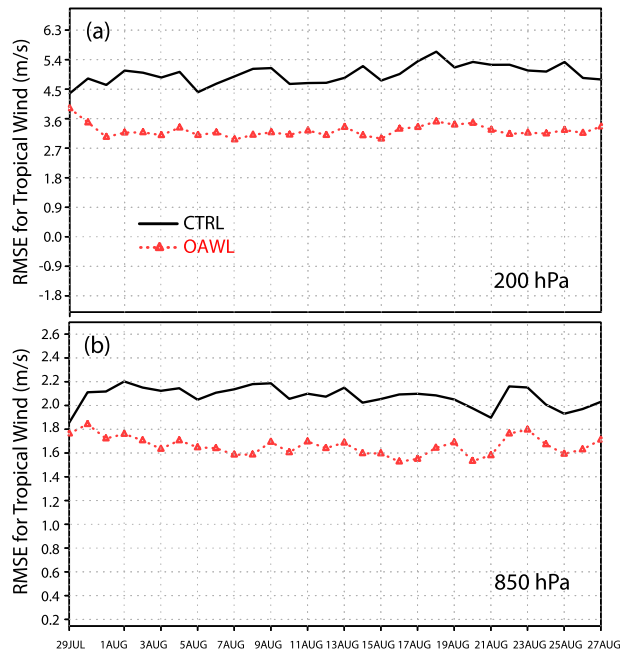


FIG. 9. The RMSE (vs the T511 NR,  $\text{m s}^{-1}$ ) for tropical ( $20^{\circ}\text{S}$ – $20^{\circ}\text{N}$ ) wind analyses at (a) 200 and (b) 850 hPa for CTRL (black) and OAWL (red) from 29 Jul to 27 Aug 2005.

### b. Experimental setup

OAWL observations were simulated from the HNR1 for three synoptic times (i.e., for 18 h) centered on the analysis times of 0600, 1200, and 1800 UTC 4 Aug 2005, which is the critical time period of rapid intensification. These observations were simulated from the highest-resolution grid of the HNR1 available for the observation location and time. The resulting data coverage is shown in Fig. 16. Note that GSI thins data as dense as the OAWL data and that it ignores locations near and outside of the HWRF boundary.

Results from six experiments are compared here. We name these experiments according to what data are assimilated in the global (g) and regional (r) domains. The first three—all of which use IC from the global CTRL OSSE analyses and BC from the global CTRL OSSE forecasts, all interpolated to the HWRF outer domain grid—are as follows:

- 1) *gCTRL*: a series of cold start forecasts from the global CTRL OSSE analyses.
- 2) *gCTRL+rCTRL*: a control DA experiment that uses the HWRF GSI DA system to assimilate the control set of conventional and satellite observations (described above in section 4b).
- 3) *gCTRL+rOAWL*: a DA experiment that parallels *gCTRL+rCTRL* but with the addition of the OAWL data simulated from HNR1 using enhanced aerosol profiles.

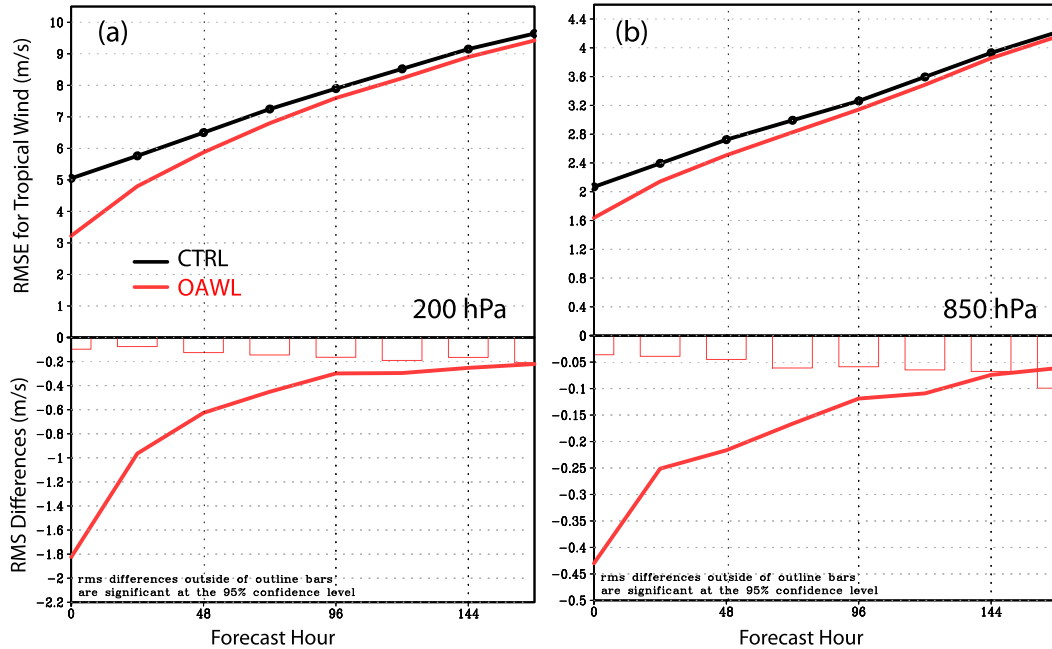


FIG. 10. The RMSE ( $\text{m s}^{-1}$ ) for tropical ( $20^{\circ}\text{S}$ – $20^{\circ}\text{N}$ ) wind forecasts initialized at 0000 UTC at (a) 200 and (b) 850 hPa for the period 7–27 Aug 2005 for CTRL (black) and OAWL (red). In this type of plot, the top panel compares the statistics from the two experiments and the bottom panel plots the difference of the statistics of the experiments. In the bottom panel, the error bars correspond to differences that are significant at the 95% confidence level.

To start the gCTRL+rCTRL experiment, the global CTRL OSSE analysis provides the IC at 0000 UTC 1 August 2005 needed to create the first background forecast. Then gCTRL+rOAWL branches off from gCTRL+rCTRL at 0600 UTC 4 August 2005.

Three additional experiments have identical configurations as gCTRL, gCTRL+rCTRL, and gCTRL+rOAWL, except that the global OAWL OSSE analyses and forecasts are used for IC and BC. These experiments, collectively the global OAWL experiments, are named gOAWL, gOAWL+rCTRL, and gOAWL+rOAWL, respectively. An interesting aspect that we can address with the global OAWL experiments is, what is the impact of assimilating the lidar data globally on the HWRF forecast?

All these experiments use the 2012 version of the operational NCEP HWRF DA system. This system is similar to the GDAS described in section 4b, with HWRF replacing GFS. The relationship of the outer and inner HWRF domains to the HNR1 outer domain is shown in Fig. 16. The outer domain has 61 vertical levels and a 9-km horizontal grid of  $708 \times 412$  grid points. The GSI analysis is computed on the outer domain, and analysis increments are interpolated to and added to the inner domain. The inner domain follows the storm and has a 3-km horizontal grid of  $352 \times 340$  grid points.

c. Preliminary results

Firm conclusions cannot be drawn from only three initial times for a single hurricane; however, these three times occur during the rapid intensification of this hurricane and so are of great interest. It should also be noted that the HWRF DA system of 2012 provided an initial operational capability and that in 2013 and 2014 the system has matured and become more accurate. Hence, results presented in this section are preliminary and we present only selected results to show the potential of experiments of this type.

1) DOMAINWIDE WIND AND SURFACE PRESSURE ERROR STATISTICS

In the regional HWRF experiment forecasts, the average SLP RMS errors over the HWRF outer (9 km) domain show a substantial improvement, except at 6 h, of the gCTRL+rOAWL experiment over the gCTRL+rCTRL experiment (not shown).

2) FORECAST TRACKS

Figure 17 shows the HNR1 best track (in black) along with the OSSE forecast tracks. Notably all the forecast tracks are west of the best track. The gCTRL and gOAWL forecast tracks are closest to the best track, but in these forecasts the hurricane moves more quickly than in the NR. Except for the gCTRL+rCTRL forecast at 0600 UTC, the

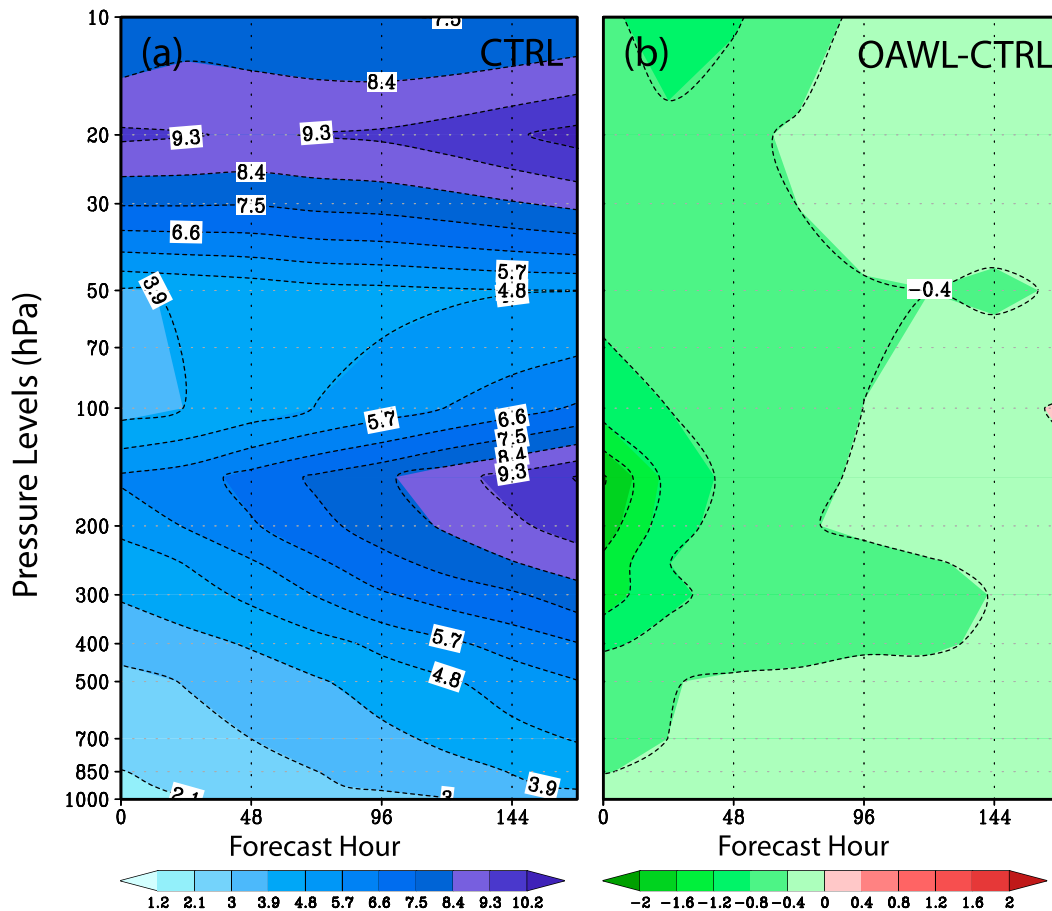


FIG. 11. The (a) RMSE ( $\text{m s}^{-1}$ ) for tropical ( $20^{\circ}\text{S}$ – $20^{\circ}\text{N}$ ) wind forecasts initialized at 0000 UTC for the period 7–27 Aug 2005 for CTRL and (b) RMSE difference (OAWL minus CTRL). In this type of plot, the statistics are shown as a function of forecast time (h) and pressure level (hPa). In (b) and similar panels in Fig. 13 showing the difference of the statistics (experiment minus control), red areas denote a negative impact and green areas a positive impact of the experimental treatment.

gCTRL+rOAWL and gOAWL+rOAWL forecasts tracks are farthest from the best track and turn more strongly to the east during the last 24–30 h of the forecast.

### 3) AVERAGE HURRICANE TRACK AND INTENSITY ERRORS

Figure 18 shows the impact of the global assimilation of OAWL data on hurricane track and intensity predictions using HWRF and compares the relative accuracy of HWRF forecasts resulting from either global or regional assimilation of OAWL data. The average errors are plotted as colored lines with matching symbols every 6 h when we have the tracker data. For the small sample of forecasts available, claims of statistical significance are not possible. Instead, we show the range of forecast error about each average error by semitransparent shading in Fig. 18.

Comparing gOAWL and gCTRL results, it is seen that the global assimilation of OAWL data improves

track forecasts substantially after 36 h (Fig. 18a), while it improves intensity forecasts for the first 60 h (Fig. 18b). Comparing gOAWL and gCTRL+rOAWL results shows that the improvement of boundary conditions for the HWRF regional model in gOAWL has a significantly larger impact on track forecast accuracy than does the regional assimilation of DWL data in gCTRL+rOAWL (Fig. 18c). In contrast, regional assimilation has a significantly larger impact on the forecast of maximum wind (Fig. 18d).

## 6. Concluding remarks

The objectives of the OSSEs described in this study are to evaluate the potential impact of a new observing system—the optical autocovariance wind lidar (OAWL)—on NWP predictions, including hurricane track and intensity predictions. To this end, we

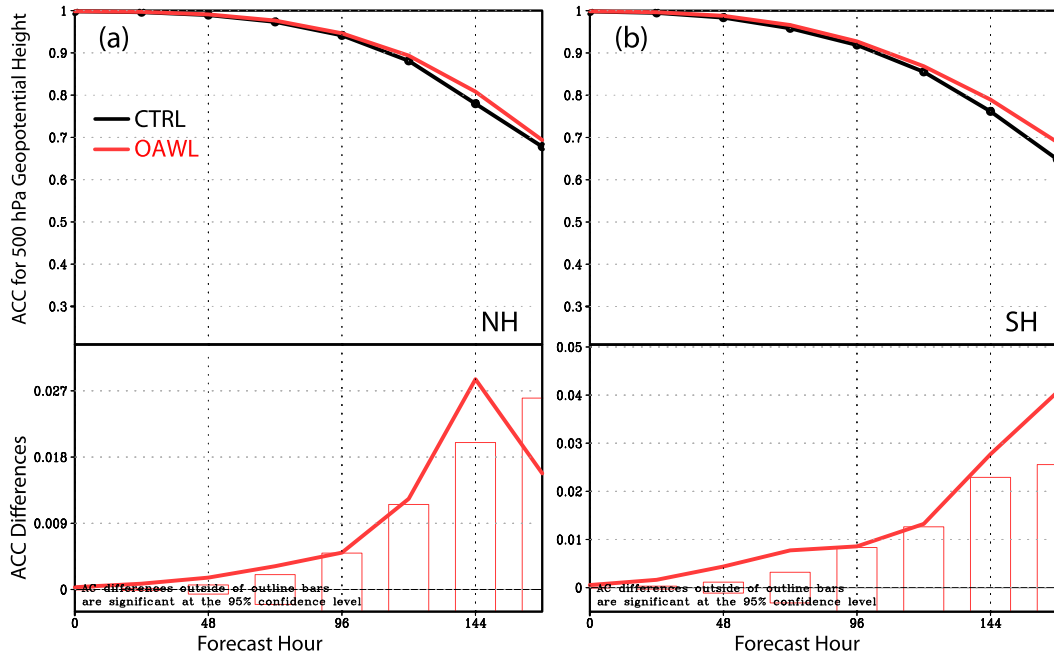


FIG. 12. As in Fig. 10, except the ACC (unitless) for (a) NH and (b) SH extratropical (20°–80°N/S) 500-hPa geopotential height forecasts initialized at 0000 UTC for the period 7–27 Aug 2005 for CTRL (black) and OAWL (red).

developed a conceptual instrument model for OAWL; generated unique very realistic simulations of OAWL data from the global T511 NR and the embedded HNR1; performed an extensive lidar data product

evaluation; and performed OSSEs using state-of-the-art (circa 2012) global and regional OSSE systems. The most general conclusion from this study is that the OAWL instrument operating at 355 nm would be

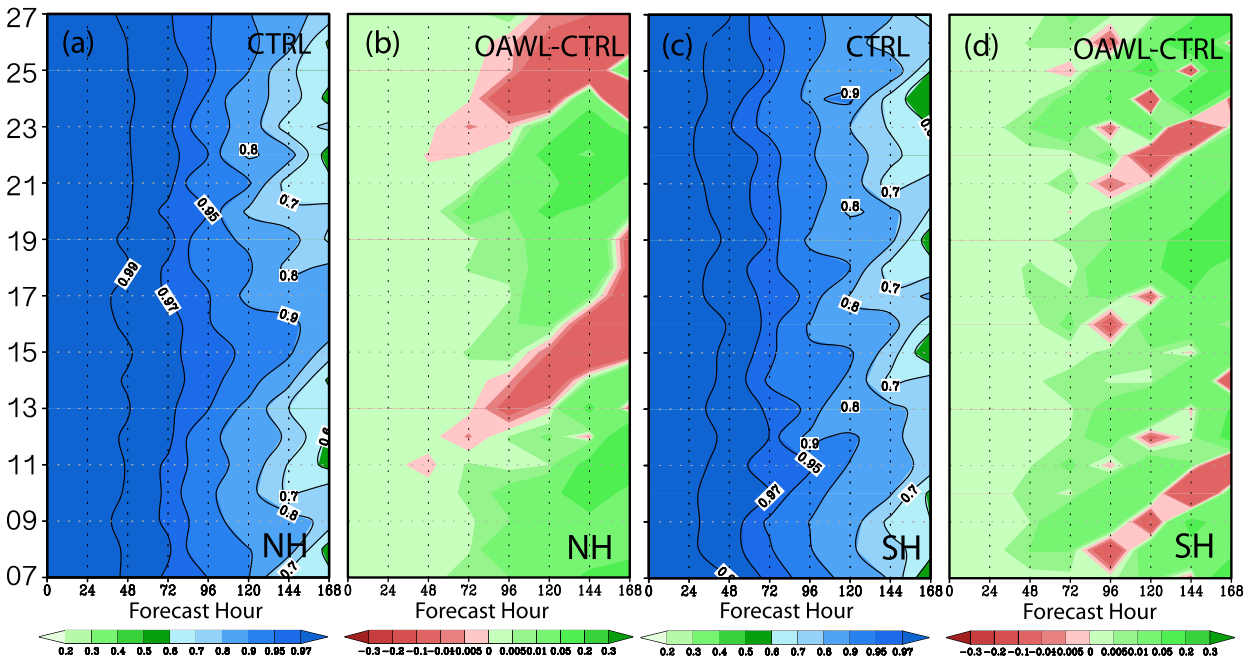


FIG. 13. The ACC (unitless) for (a),(b) NH and (c),(d) SH extratropical (20°–80°N/S) 500-hPa geopotential height forecasts initialized at 0000 UTC for the period 7–27 Aug 2005 for (a),(c) CTRL and (b),(d) OAWL minus CTRL. As in Fig. 11, but plotted as a function of forecast time (h) and verification day in August 2005.

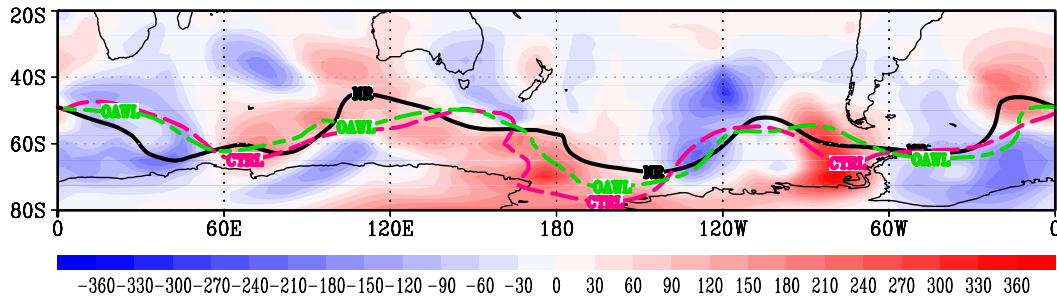


FIG. 14. The CTRL minus OAWL difference of 7-day 500-hPa geopotential height forecasts initialized 0000 UTC 19 Aug 2005. A single contour of geopotential height at 5100 m is shown for the full field from the NR (black) and experiments CTRL (magenta) and AOWL (green).

capable of making significant improvements to atmospheric analyses and numerical forecasts.

*a. Main results*

Both global and regional OSSEs demonstrate significant potential for lidar wind profile observations from

space to improve global NWP and hurricane track and intensity prediction. In the global experiments that were run, we used the ECMWF T511 NR and the GFS at T382 to perform DA. The control assimilation includes all the 2012 observing systems that were then used operationally. The OAWL experiment adds the OAWL

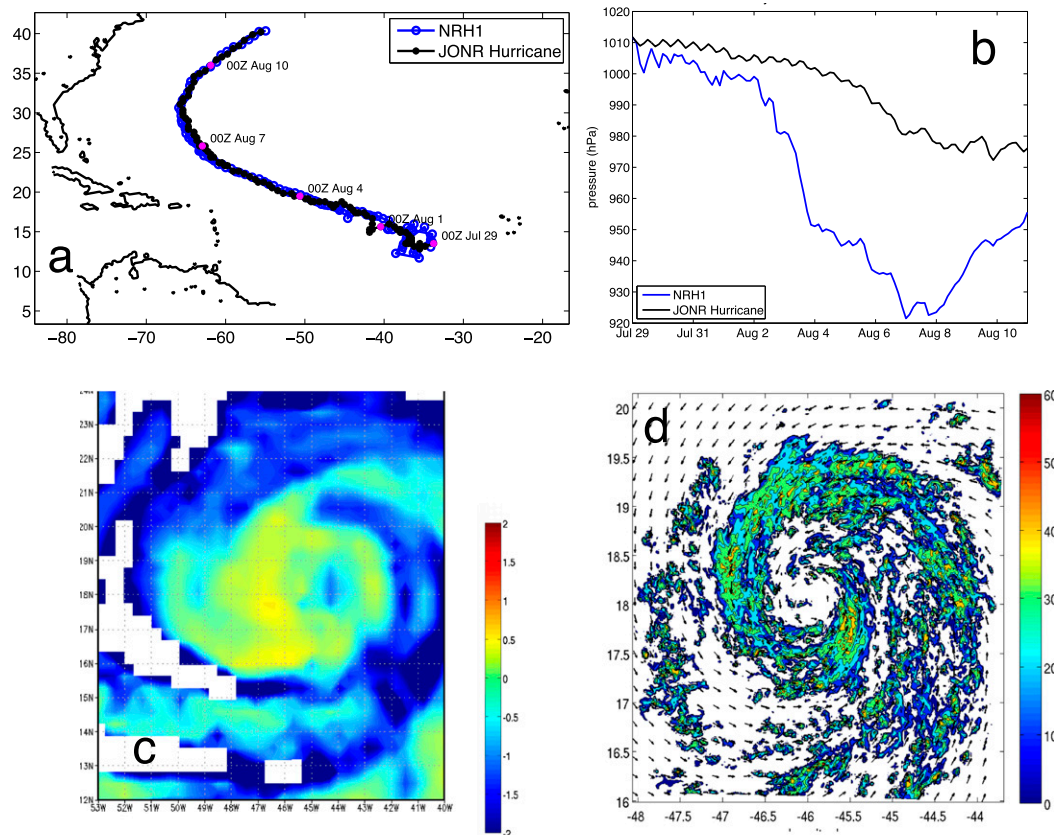


FIG. 15. The (a) track and (b) minimum surface pressure in HNR1 and T511 NR as a function of time and representations of precipitation for (c) the T511 NR and (d) the HNR1. In (a) and (b), values are plotted every 3 h, and the data for the HNR1 are from the 1-km grid, adjusted to 60-s means. Locations of the T511 NR hurricane corresponding to the dates shown are marked in magenta. Panels (a) and (b) are after Nolan et al. (2013, Fig. 4), and panel (d) is similar to Nolan et al. (2013, Figs. 5–7) but for a different time.



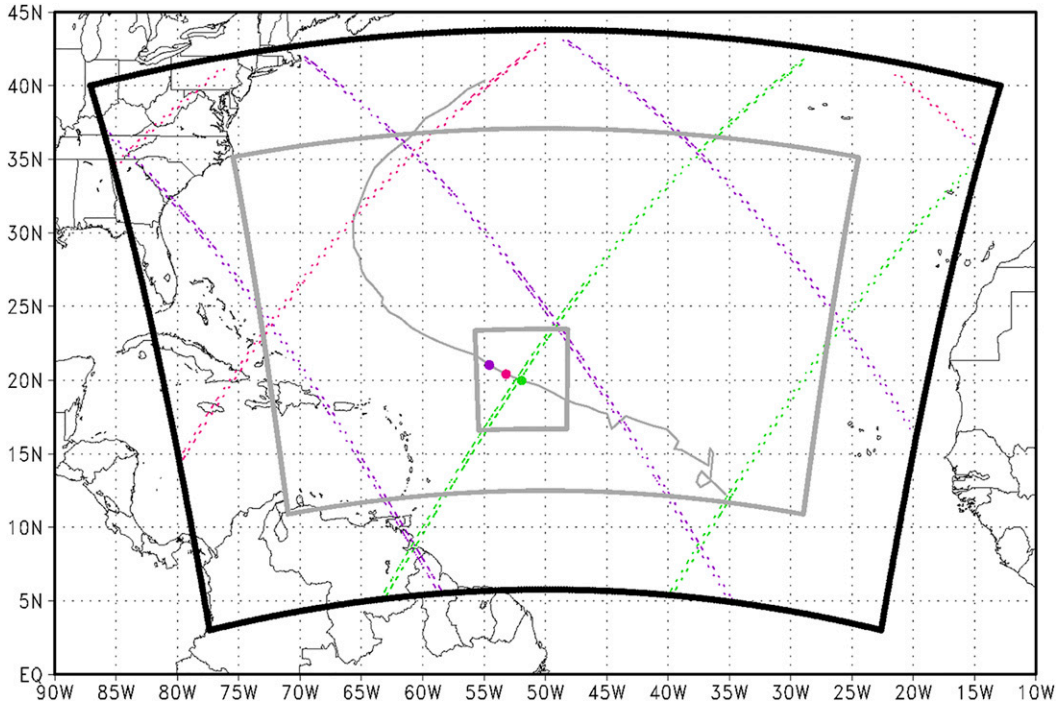


FIG. 16. Model domains, storm track, and OAWL locations for the regional OSSEs. The model domains shown include the HNR1 outer domain in black, and the HWRF inner and outer domains in gray. Note that HWRF inner domain moves with the hurricane and is here pictured at 0600 UTC 4 Aug 2005. For reference the HNR1 storm track is shown for 0000 UTC 1–11 Aug 2005, with green-, red-, and purple-filled circles at 0600, 1200, and 1800 UTC 4 Aug 2005, respectively. The OAWL locations are plotted as dots using the same color scheme. The number of OAWL observations simulated (used in the GSI) is 4460 (2385) at 0600 UTC, 2880 (982) at 1200 UTC, and 6600 (3378) at 1800 UTC 4 Aug 2005.

data. In each experiment we cycle through the DA and produce forecasts. In the parallel regional OSSEs, the ARW provides the NR.

For the wind analysis accuracy in the tropics in the global OSSEs, the addition of OAWL improves the

analysis accuracy very significantly. For 200-hPa tropical winds, the analysis RMSE is reduced from approximately 5.0 to approximately 3.25  $\text{m s}^{-1}$ , a reduction of error variance of 57%. Similarly, in the forecasts for wind in the tropics, there are substantial, statistically

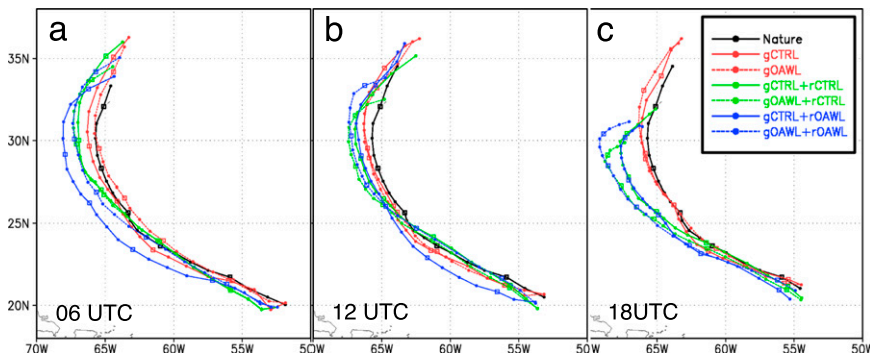


FIG. 17. Best track and forecast tracks of the regional OSSEs for initial times of (a) 0600, (b) 1200, and (c) 1800 UTC 4 Aug 2005. The HNR1 best track is in black. Tracks for experiments with global CTRL IC and BC are drawn with solid lines and experiments with global OAWL IC and BC are drawn with dotted lines. Red, green, and blue lines indicate experiments gCTRL, gCTRL+rCTRL, and gCTRL+rOAWL, respectively, as well as experiments gOAWL, gOAWL+rCTRL, and gOAWL+rOAWL, respectively.

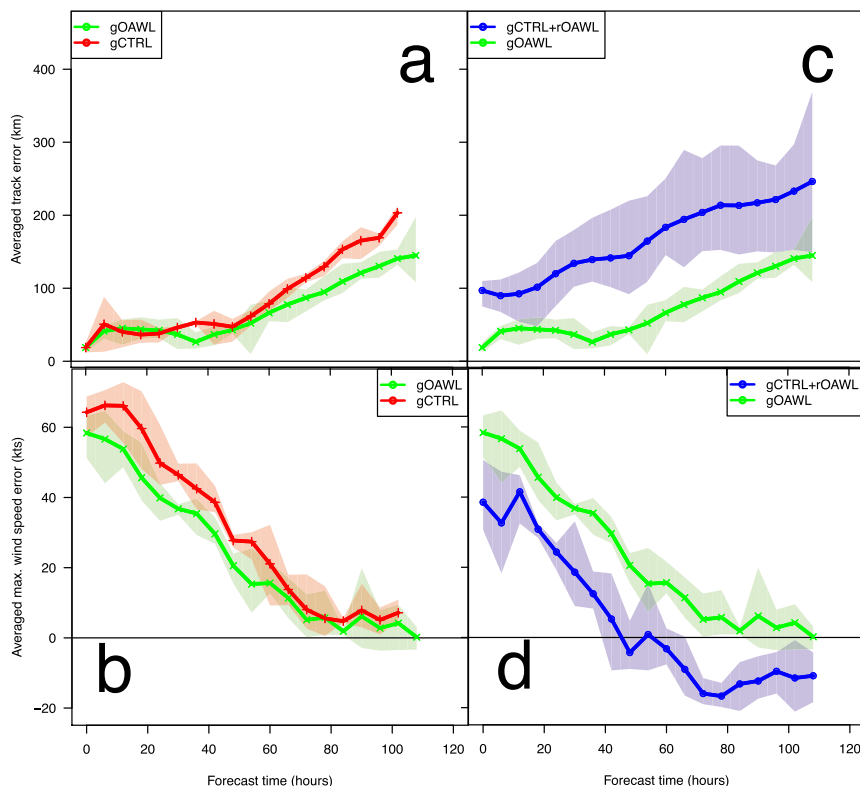


FIG. 18. Average errors for (a),(c) track (km) and (b),(d) maximum wind speed (kt;  $1 \text{ kt} = 0.51 \text{ m s}^{-1}$ ) as a function of forecast time for experiments (a),(b) gOAWL and gCTRL and (c),(d) gCTRL+rOAWL and gOAWL. The average is over the three synoptic times shown in Fig. 17. Shading shows the range of errors at each synoptic time for each experiment. Toward the end of the forecast period, points are no longer plotted when a storm center cannot be identified by the vortex tracker in each of the three forecasts for that experiment.

significant improvements from OAWL data. All tropical wind forecasts in our sample are improved (Fig. 11). The OAWL experiment also demonstrated the beneficial impact on the extratropics' 500-hPa height forecasts. At forecast hour 144 (day 6), the OAWL impact on the 500-hPa anomaly correlation coefficient (ACC) is a statistically significant improvement of approximately 2.8% and 2.9% in the Northern and Southern Hemisphere extratropics, respectively (Fig. 12). This OSSE did show considerable case-to-case variability, with examples of negative and positive impact of OAWL relative to the control in the extratropics (reddish hues in Fig. 13 are negative impacts).

In the limited HWRf forecast experiments that we have performed thus far, the assimilation of OAWL data on the global scale (gOAWL vs gCTRL) had a substantial positive impact on the track forecast, while the assimilation of OAWL data on the regional scale (gCTRL+rOAWL vs gOAWL) had a substantial positive impact on the intensity forecast. In particular,

improving the HWRf IC and BC by adding OAWL data to the global assimilation has a beneficial impact in the gOAWL experiment, compared to the gCTRL experiment, on both the HWRf track and intensity forecasts. Also, including OAWL data in the regional DA (gCTRL+rOAWL) resulted in substantially improved intensity forecasts compared to including OAWL data in the global DA (gOAWL).

#### b. Caveats

The results of these OSSEs indicate considerable potential for DWL data to improve global and hurricane forecasts, but a number of caveats must be accounted for in interpreting the experimental results. First, the sample sizes are small, especially for the regional OSSEs. More cases would provide greater statistical significance. Second, realistic errors should be used next for simulating the CTRL experiment observations. Adding such errors might be expected to make the DWL data even more valuable. Third, our 2012 operational DA

and forecast systems have been replaced by more advanced, and in the case of the GDAS, higher-resolution systems. The 2015 operational systems now use a hybrid ensemble Kalman filter (EnKF) and GSI analysis, which makes use of improved forecast error covariances. The hybrid DA system is expected to improve analyses and forecasts, including those for hurricanes. It is possible that in a hybrid DA system, more information will be extracted from the OAWL data, especially in the tropics, where geostrophy is not used in the nonhybrid GSI static covariances. Further development of the OSSE system is warranted, and is in fact underway. Fourth, the current experiments use only the background aerosol and only observations from the OAWL technique. There will be more accurate OAWL data with enhanced aerosol and there will be more OAWL data if the double-edge (molecular) detector data are used. Both of these changes are expected to increase the positive impact of OAWL. Additional bracketing experiments are called for. Fifth, the current study is largely confined to statistical metrics. Additional study of large impact cases should illuminate the mechanisms whereby the OAWL data produce positive impacts.

### c. Outlook

We are currently developing a new OSSE system, with new NRs and with more up-to-date DA components. In the future, additional OSSEs may be used to evaluate trade-offs in the design and configuration of the OAWL DWL or of other proposed observing systems and to optimize sampling strategies for current and future airborne and space-based DWLs or other observing systems. In particular, further experiments on different technologies for DWL, both on aircraft and in LEO, are planned. In addition OSSEs can be used to evaluate and improve DA methods, such as different vortex initialization methodologies based on sparse and incomplete DWL profiles and other in-storm observing systems for application to hurricane forecasting.

*Acknowledgments.* The following scientists supported the principal investigator and coinvestigators in the performance of this project and made very significant contributions to this study: Tomislava Vukicevic, Altug Aksoy, Javier Delgado, Sundara Gopalakrishnan, and Xuejin Zhang at NOAA's Atlantic Oceanographic and Meteorological Laboratory; Lars Peter Riishojgaard at the World Meteorological Organization, Geneva, Switzerland; Jack Woollen and Michiko Masutani at the Joint Center for Satellite Data Assimilation; Bob Rosenberg, Tom Clune, Eric Kemp, Juan-Carlos Jusem, and Josse Jacob at NASA's Goddard Space Flight Center; and Sharan Majumdar, David Nolan, and Brian

McNoldy at the University of Miami's Rosenstiel School of Marine and Atmospheric Science. This research was supported by NASA's Earth Science Technology Office (ESTO) and by NOAA's Office of Weather and Air Quality (OWAQ). We especially thank Michael Seabloom of NASA headquarters and John Cortinas of OWAQ for their support. This research was carried out in part under the auspices of the Cooperative Institute for Marine and Atmospheric Studies (CIMAS), a Cooperative Institute of the University of Miami and the National Oceanic and Atmospheric Administration, Cooperative Agreement NA10OAR4320143, with funding from Award NA14OAR4830103, "CIMAS Contributions to OAR Disaster Recovery Act Projects." We thank the reviewers for their careful and helpful reviews.

### REFERENCES

- Aksoy, A., S. Lørsolo, T. Vukićević, K. J. Sellwood, S. D. Aberson, and F. Zhang, 2012: The HWRP Hurricane Ensemble Data Assimilation System (HEDAS) for high-resolution data: The impact of airborne Doppler radar observations in an OSSE. *Mon. Wea. Rev.*, **140**, 1843–1862, doi:10.1175/MWR-D-11-00212.1.
- Andersson, E., and M. Masutani, 2010: Collaboration on observing system simulation experiments (joint OSSE). *ECMWF Newsletter*, No. 123, ECMWF, Reading, United Kingdom, 14–16.
- Atlas, R., 1997: Atmospheric observations and experiments to assess their usefulness in data assimilation. *J. Meteor. Soc. Japan*, **75**, 111–130.
- , and L. P. Riishojgaard, 2008: Application of OSSEs to observing system design. *Remote Sensing System Engineering*, P. E. Ardanuy, and J. J. Puschell, Eds., International Society for Optical Engineering (SPIE Proceedings, Vol. 7087), 708707, doi:10.1117/12.795344.
- , E. Kalnay, W. E. Baker, J. Susskind, D. Reuter, and M. Halem, 1985a: Simulation studies of the impact of future observing systems on weather prediction. Preprints, *Seventh Conf. on Numerical Weather Prediction*, Montreal, QC, Canada, Amer. Meteor. Soc., 145–151.
- , —, and M. Halem, 1985b: Impact of satellite temperature soundings and wind data on numerical weather prediction. *Opt. Eng.*, **24**, 242341, doi:10.1117/12.7973481.
- , and Coauthors, 2001: The effects of marine winds from scatterometer data on weather analysis and forecasting. *Bull. Amer. Meteor. Soc.*, **82**, 1965–1990, doi:10.1175/1520-0477(2001)082<1965:TEOMWF>2.3.CO;2.
- Baker, W. E., and Coauthors, 2014: Lidar-measured wind profiles: The missing link in the global observing system. *Bull. Amer. Meteor. Soc.*, **95**, 543–564, doi:10.1175/BAMS-D-12-00164.1.
- Bruneau, D., 2001: Mach-Zehnder interferometer as a spectral analyzer for molecular Doppler wind lidar. *Appl. Opt.*, **40**, 391–399, doi:10.1364/AO.40.000391.
- , 2002: Fringe-imaging Mach-Zehnder interferometer as a spectral analyzer for molecular Doppler wind lidar. *Appl. Opt.*, **41**, 503–510, doi:10.1364/AO.41.000503.
- , and J. Pelon, 2003: Simultaneous measurements of particle backscattering and extinction coefficients and wind velocity by lidar with a Mach-Zehnder interferometer: Principle of

- operation and performance assessment. *Appl. Opt.*, **42**, 1101–1114, doi:10.1364/AO.42.001101.
- , A. Garnier, A. Hertzog, and J. Porteneuve, 2004: Wind velocity lidar measurements by use of a Mach–Zehnder interferometer, comparison with a Fabry–Perot interferometer. *Appl. Opt.*, **43**, 173–182, doi:10.1364/AO.43.000173.
- , F. Blouzon, J. Spatazza, F. Montmessin, J. Pelon, and B. Faure, 2013: Direct-detection wind lidar operating with a multimode laser. *Appl. Opt.*, **52**, 4941–4949, doi:10.1364/AO.52.004941.
- Emmitt, G. D., 2000: Hybrid technology Doppler wind lidar: Assessment of simulated data products for a space-based system concept. *Lidar Remote Sensing for Industry and Environment Monitoring*, U. N. Singh, T. Itabe, and N. Sugimoto, Eds., International Society for Optical Engineering (SPIE Proceedings, Vol. 4153), 366, doi:10.1117/12.417069.
- , 2001: Updated report on hybrid technology DWLs. *Proc. Working Group on Space-Based Lidar Winds*, Oxnard, CA, NOAA, 13 pp. [Available online at <http://cires1.colorado.edu/events/lidarworkshop/LWG/Feb01/Papers.feb01/Paper10.feb01.ppt>.]
- , and S. A. Wood, 1996: Simulating clouds within a space-based Doppler lidar wind sounder simulation model. *Cloud Impacts on DoD Operations and Systems 1995 Conference (CIDOS-95)*, D. D. Grantham, Ed., Phillips Laboratory, Hanscom Air Force Base, Environmental Research Papers 1179, PL-TR-95-2129, 69–71.
- , and —, 2003: Status of hybrid DWL study. *Proc. Working Group on Space-Based Lidar Winds*, Oxnard, CA, NOAA, 17 pp. [Available online at <http://cires1.colorado.edu/events/lidarworkshop/LWG/Feb03/Papers.feb03/Emmitt2.feb03.ppt>.]
- , and —, 2011: Performance characteristics and design trades for an ISS hybrid Doppler wind lidar. *Proc. Working Group on Space-Based Lidar Winds*, Miami, FL, NOAA, 48 pp. [Available online at <http://cires1.colorado.edu/events/lidarworkshop/LWG/Feb11/ISSPapers.feb11/Emmitt1.feb11.pptx>.]
- , J. Spinhirne, R. Menzies, D. Winker, and D. Bowdle, 2001: Target atmospheres for use in DWL concept studies. New Millennium Program by an Ad Hoc Committee. [Available online at <http://www.swa.com>.]
- Frehlich, R., 2000: Simulation of coherent Doppler lidar performance for space-based platforms. *J. Appl. Meteor.*, **39**, 245–262, doi:10.1175/1520-0450(2000)039<0245:SOCDLP>2.0.CO;2.
- , 2001: Errors for space-based Doppler lidar wind measurements: Definition, performance, and verification. *J. Atmos. Oceanic Technol.*, **18**, 1749–1772, doi:10.1175/1520-0426(2001)018<1749:EFSDL>2.0.CO;2.
- , 2004: Velocity error for coherent Doppler lidar with pulse accumulation. *J. Atmos. Oceanic Technol.*, **21**, 905–920, doi:10.1175/JTECH1596.
- Grund, C., and S. C. Tucker, 2011: Optical autocovariance wind lidar (OAWL): A new approach to direct-detection Doppler wind profiling. *Fifth Symp. on Lidar Atmospheric Applications*, Seattle, WA, Amer. Meteor. Soc., 4.9. [Available online at <https://ams.confex.com/ams/91Annual/webprogram/Paper188184.html>.]
- , J. Howell, R. Pierce, and M. Stephens, 2009: Optical autocovariance direct detection lidar for simultaneous wind, aerosol, and chemistry profiling from ground, air, and space platforms. *Advanced Environmental, Chemical, and Biological Sensing Technologies VI*, T. Vo-Dinh, R. A. Lieberman, and G. Gauglitz, Eds., International Society for Optical Engineering (SPIE Proceedings, Vol. 7312), 73120U, doi:10.1117/12.824204.
- Hardesty, M., and Coauthors, 2005: Providing global wind profiles—The missing link in today's observing system. CIRES, 11 pp. [Available online at <http://cires1.colorado.edu/events/lidarworkshop/LWG/>.]
- Kleist, D. T., D. F. Parrish, J. C. Derber, R. Treadon, W.-S. Wu, and S. Lord, 2009: Introduction of the GSI into the NCEP Global Data Assimilation System. *Wea. Forecasting*, **24**, 1691–1705, doi:10.1175/2009WAF2222201.1.
- Liu, Z., and T. Kobayashi, 1996: Differential discrimination technique for incoherent Doppler lidar to measure atmospheric wind and backscatter ratio. *Opt. Rev.*, **3**, 47–52, doi:10.1007/s10043-996-0047-0.
- Ma, Z., L. P. Riishojgaard, M. Masutani, J. S. Woollen, and G. D. Emmitt, 2015: Impact of different satellite wind lidar telescope configurations on NCEP GFS forecast skill in observing system simulation experiments. *J. Atmos. Oceanic Technol.*, **32**, 478–495, doi:10.1175/JTECH-D-14-00057.1.
- McCarty, W., R. M. Errico, and R. Gelaro, 2012: Cloud coverage in the joint OSSE nature run. *Mon. Wea. Rev.*, **140**, 1863–1871, doi:10.1175/MWR-D-11-00131.1.
- Miller, T. L., and Coauthors, 2008: Simulation of the impact of new aircraft and space-based ocean surface wind measurements on H\*Wind analyses. *12th Conf. on Integrated Observing and Assimilation Systems for the Atmosphere, Oceans, and Land Surface (IOAS-AOLS)*, New Orleans, LA, Amer. Meteor. Soc., P1.6. [Available online at [https://ams.confex.com/ams/88Annual/techprogram/paper\\_133851.htm](https://ams.confex.com/ams/88Annual/techprogram/paper_133851.htm).]
- Nolan, D. S., R. Atlas, K. T. Bhatia, and L. R. Bucci, 2013: Development and validation of a hurricane nature run using the joint OSSE nature run and the WRF model. *J. Adv. Model. Earth Syst.*, **5**, 382–405, doi:10.1002/jame.20031.
- Privé, N. C., R. M. Errico, and K.-S. Tai, 2013a: The influence of observation errors on analysis error and forecast skill investigated with an observing system simulation experiment. *J. Geophys. Res. Atmos.*, **118**, 5332–5346, doi:10.1002/jgrd.50452.
- , —, and —, 2013b: Validation of the forecast skill of the Global Modeling and Assimilation Office observing system simulation experiment. *Quart. J. Roy. Meteor. Soc.*, **139**, 1354–1363, doi:10.1002/qj.2029.
- , —, and —, 2014a: The impact of increased frequency of rawinsonde observations on forecast skill investigated with an observing system simulation experiment. *Mon. Wea. Rev.*, **142**, 1823–1834, doi:10.1175/MWR-D-13-00237.1.
- , Y. Xie, S. Koch, R. Atlas, S. J. Majumdar, and R. Hoffman, 2014b: An observation system simulation experiment for the unmanned aircraft system data impact on tropical cyclone track forecasts. *Mon. Wea. Rev.*, **142**, 4357–4363, doi:10.1175/MWR-D-14-00197.1.
- Reale, O., J. Terry, M. Masutani, E. Andersson, L. P. Riishojgaard, and J. C. Jusem, 2007: Preliminary evaluation of the European Centre for Medium-Range Weather Forecasts' (ECMWF) Nature Run over the tropical Atlantic and African monsoon region. *Geophys. Res. Lett.*, **34**, L22810, doi:10.1029/2007GL031640.
- Riishojgaard, L. P., Z. Ma, M. Masutani, J. S. Woollen, G. D. Emmitt, S. A. Wood, and S. Greco, 2012: Observation system simulation experiments for a global wind observing sounder. *Geophys. Res. Lett.*, **39**, L17805, doi:10.1029/2012GL051814.

- Schwiesow, R. L., and S. D. Mayor, 1995: Coherent optical signal processing for a Doppler lidar using a Michelson interferometer, coherent laser radar. *Coherent Laser Radar: Summaries of the Papers Presented at the Topical Meeting*, Technical Digest Series, Vol. 19, OSA, 212–215.
- Stauffer, D. R., and N. L. Seaman, 1990: Use of four-dimensional data assimilation in a limited-area mesoscale model. Part I: Experiments with synoptic-scale data. *Mon. Wea. Rev.*, **118**, 1250–1277, doi:[10.1175/1520-0493\(1990\)118<1250:UOFDDA>2.0.CO;2](https://doi.org/10.1175/1520-0493(1990)118<1250:UOFDDA>2.0.CO;2).
- , —, and F. S. Binkowski, 1991: Use of four-dimensional data assimilation in a limited-area mesoscale model. Part II: Effects of data assimilation within the planetary boundary layer. *Mon. Wea. Rev.*, **119**, 734–754, doi:[10.1175/1520-0493\(1991\)119<0734:UOFDDA>2.0.CO;2](https://doi.org/10.1175/1520-0493(1991)119<0734:UOFDDA>2.0.CO;2).
- Tucker, S., and C. Weimer, 2013: Comparing and contrasting the Optical Autocovariance Wind Lidar (OAWL) and coherent detection lidar. *Proc. 17th Coherent Laser Radar Conf. (CLRC 2013)*, Barcelona, Spain, Universities Space Research Association, 50–53. [Available online at [http://www.tsc.upc.edu/clrc/wp-content/uploads/Manuscripts/clrc2013\\_submission\\_19.pdf](http://www.tsc.upc.edu/clrc/wp-content/uploads/Manuscripts/clrc2013_submission_19.pdf).]
- Wood, S. A., Jr., G. D. Emmitt, and S. Greco, 2000: DLSM: A coherent and direct detection lidar simulation model for simulating space-based and aircraft-based lidar winds. *Laser Radar Technology and Applications V*, G. W. Kamerman et al., Eds., International Society for Optical Engineering (SPIE Proceedings, Vol. 4035), 2, doi:[10.1117/12.397788](https://doi.org/10.1117/12.397788).
- , —, and —, 2001: The challenges of accessing the future impact of space-based Doppler wind lidars while using today's global and regional atmospheric models. Preprints, *Fifth Symp. on Integrated Observing Systems*, Albuquerque, NM, Amer. Meteor. Soc., P1.5. [Available online at <https://ams.confex.com/ams/annual2001/webprogram/Paper18512.html>.]
- Zhang, L., and Z. Pu, 2010: An observing system simulation experiment (OSSE) to assess the impact of Doppler wind lidar (DWL) measurements on the numerical simulation of a tropical cyclone. *Adv. Meteor.*, **2010**, 743863, doi:[10.1155/2010/743863](https://doi.org/10.1155/2010/743863).